PDE and Jitter modelling of SPAD Devices.

Rémi Helleboid[1], Denis Rideau[1], Isobel Nicholson[2], Norbert Moussy[3], Olivier Saxod[3], Jeremy Grebot[1], Antonin Zimmerman[1], Sara Pellegrini[2], and Matthieu Sicre[1]

[1] *ST Microelectronics, Crolles, France*
[2] *ST Microelectronics, Edinburgh, UK*
[3] *CEA LETI, Grenoble, France*

Abstract

In this paper we present a full 3D simulation methodology to extract Photon Detection Probability (PDP) and Jitter of Single-Photon Avalanche Diode (SPAD) Devices. The simulation results are compared with measurements on devices and show good agreement with the experiments.

Keywords— single-photon avalanche diode (SPAD), photon detection probability (PDP), jitter, avalanche breakdown probability, breakdown voltage

1 Introduction

Single Photon Avalanche Diodes (SPAD) are key optoelectronic detectors for medical imaging, camera ranging and automotive laser imaging detection and ranging (LiDAR) applications. Currently, the device leading the market is a micrometric silicon (Si) PN junction associated to a proximity CMOS electronics biasing the system above the breakdown voltage. Si-SPADs present low noise and relatively high photon detection probability (PDP), but their sensitivity is limited to photon wavelengths lower than 1100 nm, while class 1 eye-safety devices would require wavelengths larger than 1400 nm.

2 Device structure and TCAD simulation

A variety of SPAD architectures were devised with pitch size ranging from five to ten microns. Each layout was devised to create a different electric field profile which can vary both laterally and vertically through the full volume of the device. These architectures were manufactured on silicon and characterized using a methodology which prevents contamination of results from any potential crosstalk.
The structures' doping profiles were modelled with a well-calibrated process simulator followed by electrostatic device simulation. The resulting electric field profiles (calculated as usual by the solution of the Poisson equation) were used as the starting point for a suite of in-house softwares developed to calcuate breakdown probability and jitter characteristics. The carrier density ρ and the recombination-generation processes were computed by resolving current continuity equations consistently with the drift-diffusion transport model.
In parallel, optical simulation with a well-known FDTD solver was performed on the architectures to obtain maps of optical absorption. The back end of the devices including the microlens and texturation was kept constant for each comparison.

3 Avalanche breakdown probability

The avalanche breakdown probability is computed by the means of the well known McIntyre model [1]. We briefly recall the model derivation : Let $P_e(x)$ be the probability that an electron starting at x in the depletion layer triggers an avalanche and $P_h(x)$ the same probability for an hole starting at x. Straightforwardly, the probability that neither an hole nor an electron starting at x trigger an avalanche is given by $(1-P_e(x))(1-P_h(x))$. Thus, the probability that either the hole or the electron trigger an avalanche, noted P_{pair} is :

$$\begin{aligned} P_{pair}(x) &= 1-(1-P_e(x))\left(1-P_h(x)\right) \\ &= P_e+P_h-P_eP_h \end{aligned}$$

Now, the probability that an electron starting at $x+dx$ triggers an avalanche is : The probability that the electron reaches the position x and triggers an avalanche in x plus the probability that it triggers an avalanche between x and $x+dx$ less the probability of the intersection of the two previous events. It writes :

$$\begin{aligned} P_e(x+dx) &= P_e(x)+\alpha_e(x)dxP_{pair}(x)-P_e(x)\alpha_e dxP_{pair}(x) \\ &= P_e(x)+\alpha_e(x)dx(P_e(x)+P_h(x)-P_e(x)P_h(x)) \\ &\quad -P_e(x)\alpha_e(x)dx(P_e(x)+P_h(x)-P_e(x)P_h(x)) \\ &= P_e(x)+dx\,\alpha_e(x)(P_e(x)+P_h(x)-P_e(x)P_h(x))(1-P_e(x)) \end{aligned}$$

Where α_e is the electron linear ionization rate : the probability by length that an electron create an impact ionization event.
One can rearrange the terms to obtain :

$$\frac{P_e(x+dx)-P_e(x)}{dx}=\alpha_e(x)(P_e(x)+P_h(x)-P_e(x)P_h(x))(1-P_e(x))$$

Which leads to the first ordinary differential equation :

$$\frac{dP_e}{dx}=(1-P_e)\alpha_e(P_e+P_h-P_eP_h)$$

The same reasoning applies to the probability that an hole starting at $x-dx$ triggers an avalanche. Which leads to the second ordinary differential equation :

$$\frac{dP_h}{dx}=-(1-P_h)\alpha_h(P_e+P_h-P_eP_h)$$

Therefore we can draw up the McIntyre system :

$$\begin{cases} \dfrac{dP_e}{dx}=(1-P_e)\alpha_e(P_e+P_h-P_eP_h) & (1) \\ \dfrac{dP_h}{dx}=-(1-P_h)\alpha_h(P_e+P_h-P_eP_h) & (2) \end{cases}$$

for $0\le x\le W$.
Adding the couple of boundary value conditions :

$$\begin{cases} P_e(x=0)=0 & (3) \\ P_h(x=W)=0 & (4) \end{cases}$$

we have a full 1D coupled and non-linear boundary value problem. Since we have to extract this value at a large number of points, we use a self-made solver, embedded in a C++ program. This solver uses finite difference method coupled with a Newton's method to care of the non-linearity of the problem [2].

3.1 Newton's method

We set the following notations :

$$Y(x) = \begin{pmatrix} P_e(x) \\ P_h(x) \end{pmatrix}$$

$$f(Y,x) = \begin{pmatrix} (1-Y_1(x))\alpha_e(Y_1(x)+Y_2(x)-Y_1(x)Y_2(x)) \\ -(1-Y_2(x))\alpha_h(Y_1(x)+Y_2(x)-Y_1(x)Y_2(x)) \end{pmatrix}$$

$$g(s_1,s_2) = \begin{pmatrix} s_1 \\ s_2 \end{pmatrix}$$

The problem hence reads :

$$\begin{cases} Y'(x) = f(Y,x) & (5) \\ g(Y(0),Y(w)) = 0 & (6) \end{cases}$$

The numerical method relies on a finite difference method approach to discretize the problem. Let $\mathcal{M}$ be the mesh on which we work. It is given by the streamlines construction. So we have :

$$\mathcal{M} : 0 = x_1 < x_2 < x_3 < \cdots < x_N < x_{N+1} = w$$

The approximated solution on mesh $\mathcal{M}$ is $Y_{\mathcal{M}} = (y_1, y_2, \cdots, y_N, y_{N+1})$, where y_i is the approximation of $Y(x_i)$.
For numerical approximation we again consider the mesh $\mathcal{M}$ and denote the vector of approximate solution values at mesh points by $Y_{\mathcal{M}}$. The trapezoidal scheme of finite difference methods is given by :

$$\frac{y_{i+1}-y_i}{h_i} = \frac{1}{2}\left(f\left(x_{i+1},y_{i+1}\right)+f\left(x_i,y_i\right)\right) \quad 1 \le i \le N \quad (7)$$

$$g\left(y_1,y_{N+1}\right) = 0 \quad (8)$$

Thus we obtain a system of $2(N+1)$ algebraic equations for the $2(N+1)$ unknowns $Y_{\mathcal{M}}$. Unlike before, though, these equations are non-linear. The number N depends on the precision we take when we construct the streamlines. We commonly take a range of $[1nm, 10nm]$, we then have $N \sim 5000$.
We consider a system of equation written in the compact form :

$$\mathbf{F(s) = 0}$$

Then the newton method iterative method is given by the iteration :

$$\mathbf{s}^{k+1} = \mathbf{s} - \left[\mathbf{F}'(\mathbf{s})\right]^{-1}\mathbf{F}(\mathbf{s})$$

with $\mathbf{F}'(\mathbf{s})^{-1}$ the inverse of the Jacobian matrix of $\mathbf{F}$.
So the algorithm will first solve the linear system :

$$\mathbf{F}'\left(\mathbf{s}^k\right)\boldsymbol{\xi} = -\mathbf{F}\left(\mathbf{s}^k\right) \quad (9)$$

And then simply applies :

$$\mathbf{s}^{k+1} = \mathbf{s}^k + \boldsymbol{\xi} \quad (10)$$

Let $\mathbf{N}_{\mathcal{M}}$ be the following discrete differential operator :

$$\mathbf{N}_{\mathcal{M}}\mathbf{y}_i = \frac{y_{i+1}-y_i}{h_i} - \frac{1}{2}\left(f\left(x_{i+1},y_{i+1}\right)+f\left(x_i,y_i\right)\right)$$

Then

$$\mathbf{F(s)} = \left(N_{\mathcal{M}}\mathbf{y}_1, N_{\mathcal{M}}\mathbf{y}_1, \ldots, N_{\mathcal{M}}\mathbf{y}_N, g(y_1,y_{N+1})\right)$$

We set

$$\boldsymbol{\xi} = \left(\mathbf{w}_1,\mathbf{w}_2,\ldots,\mathbf{w}_N,\mathbf{w}_{N+1}\right)$$

So that the Newton method iteration becomes :

$$\frac{\mathbf{w}_{i+1}-\mathbf{w}_i}{h_i} - \frac{1}{2}\left[A\left(x_{i+1}\right)\mathbf{w}_{i+1} + A\left(x_i\right)\mathbf{w}_i\right] = -\mathbf{N}_{\mathcal{M}}\mathbf{y}_i^k \quad 1 \le i \le N \quad (11)$$

$$B_a w_1 + B_b w_{N+1} = -g\left(y_1^m, y_{N+1}^m\right) \quad (12)$$

Where A is the following matrix :

$$A\left(x_j\right) := \frac{\partial f}{\partial y}\left(x_j, \mathbf{y}_j^k\right)$$

And with

$$B_a = \frac{\partial g(\mathbf{y_1^k}, \mathbf{y_{N+1}^k})}{\partial \mathbf{u}} = 1, \quad B_b = \frac{\partial \mathbf{g}(\mathbf{y_1^k}, \mathbf{y_{N+1}^k})}{\partial \mathbf{v}} = 1$$

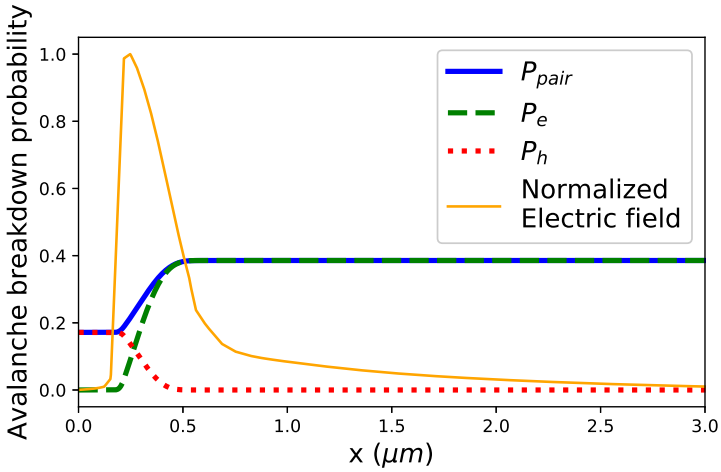

Figure 1: Typical solution of the McIntyre model for a given electric field curve

3.2 Application to field lines

The McIntyre model is a fully 1D model where the electron and holes path are assumed to be a straight line, often took from the bottom to the top of the device, see for example [3]. In this work we wish to have accurate values of breakdown probability in all the device volume. To this purpose we use electric field streamline to model the carriers transport inside the device. The field lines are computed straightforwardly using simple Euler scheme with adaptive step to ensure a good distribution of points along the line.

$$\frac{dX(s)}{ds} = \vec{F}_{electric} \quad (13)$$

Then the streamline is defined by the following set of points :

$$\{X(s) \text{ for } s \in [s_0, s_f]\}$$

Our Euler method then reads :

$$\frac{X(s+ds)-X(s)}{ds} = \vec{F}_{electric}(X(s)) \quad (14)$$

$$\Longrightarrow X(s+ds) = X(s) + \underbrace{ds\vec{F}_{electric}(X(s))}_{dX} \quad (15)$$

This operation is performed both forward (hole motion) and backward (electron motion). We then interpolate the electric field on the resulting streamline. We can now obtain a function E(x) where x is the distance from the beginning of the line and E(x) is the norm of the electric field at this point. The streamlines and this function are respectively represented on figures 2 and 1
We can now compute the impact ionization coefficients, required to compute the McIntyre's model, in this work we choose the local coefficient from Van Overstraeten and De Man [4].
We can compute the breakdown probability over multiple streamlines starting from multiple points inside the device and plot them to have an idea of the breakdown probability inside the device, see figure.

4 Jitter modeling

4.1 Drif-Diffusion model

The jitter in SPAD devices is made of multiple phenomena such as depth of photon absorption, carrier transport timing, avalanche build-up,quench circuit statistics etc.
In the present work, we focus on the modeling of the carrier transport part which is responsible for the queue of the jitter distribution. To do so, we couple the streamlines and the one dimensional advection-diffusion equation with variable velocity and diffusion. Let us consider that a photon absorption at a given point x_0 leads to the creation of an electron-hole pair, we want to simulate the timing for the electron

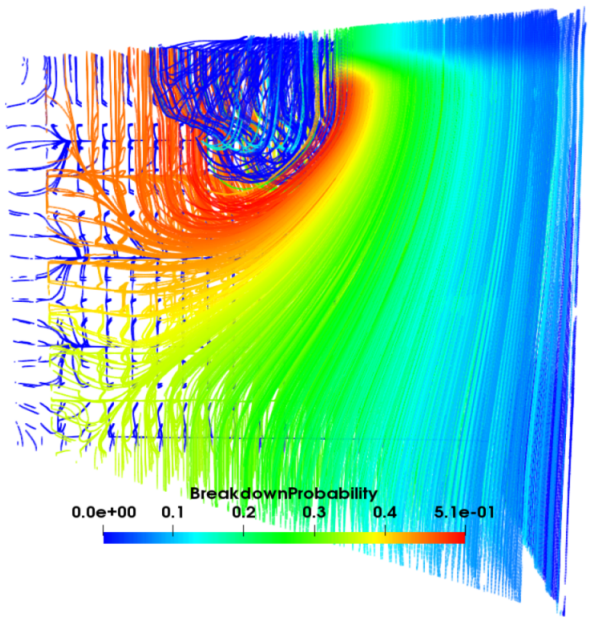

Figure 2: Breakdown Probability computed over multiple streamlines

to reach the avalanche zone, we assume that this zone is represented by the location of the maximum electric field, denoted $x_{E_{max}}$. Let $f : (x,t) \mapsto f(x,t)$ the probability distribution of an electron presence. We assume that the electron will drift and diffuse along the electric field streamline. At time $t = 0$, f is a Dirac distribution, in order to be able to compute a solution numerically, we start a time $t_0 = \delta t$ where δt is as small as possible. We then take the assumption that $D(x) = D(x_0)$ and $u(x) = u_(x_0)$, and that the analytical solution applies for a very small time interval δt.
Hence, f verify the following equation :

$$\forall x \in [x_s, x_{max}] \text{ and } t \in [t_0, T]$$

$$\frac{\partial f}{\partial t}(x,t) = -\frac{\partial (u \cdot f)}{\partial x}(x,t) + \frac{\partial}{\partial x}\left(D \cdot \frac{\partial f}{\partial x}\right)(x,t) \tag{16}$$

With the following initial condition :

$$f(x, t = t_0) = \frac{1}{\sqrt{4\pi D(x_0)\, t_0}} exp(-\frac{(x - v(x_0)\, t_0)^2}{4D(x_0)\, t_0} \tag{17}$$

And setting an absorbing boundary condition at $x_s = x_{E_{max}}$:

$$\frac{\partial f}{\partial t}(x_s,t) = \frac{\partial}{\partial x}\left(D \cdot \frac{\partial (f)}{\partial x}\right)(x_s,t) \tag{18}$$

The velocity is computed throw a high field saturation model and the diffusion throw the Einstein relation $D = \frac{\mu k_B T}{q}$, these quantities are represented in figure 3. Let T_e the time for the electron to reach the avalanche region. It is straightforward that the probability that T is less than t is:

$$P_r(t < T) = F_{Pr}(t) = 1 - \int_{x_0}^{x_{max}} f(x,t)dx$$

From this cumulative distribution function, we can find back the distribution of T:

$$f_T(t) = \frac{F_{Pr}(t)}{dt} \tag{19}$$

The equation is solved by the mean of the finite difference method, more precisely we use a modified Crank-Nicholson method that takes into account the variable velocity and diffusion.

5 Results and comparisons with experiments

To validate our models, the simulation results were compared with experimental measurements performed on the wide range of architecture

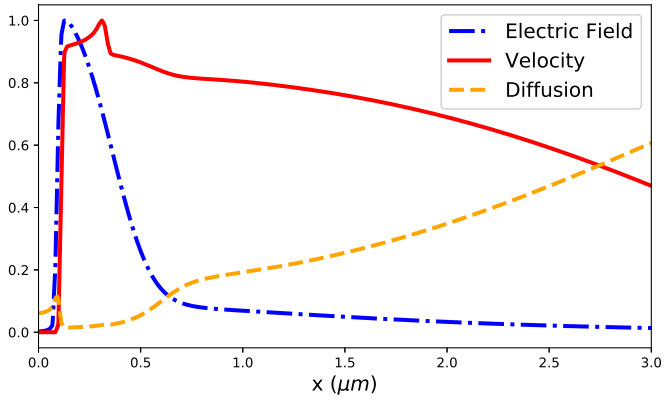

Figure 3: Normalized Electric Field, Velocity and Diffusion along a streamline

variants described in section 2. Where appropriate measurements are repeated on several SPADs to reduce the variability of the results and the values given are the median.
We first present the PDE results derived from the avalanche breakdown probability simulations described in section **??**. A key visualisation of the result is the 2D BrP colour map, which is generated for two different architectures with varying junction size in figure 4.

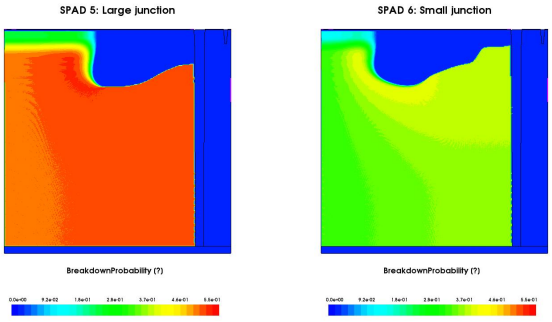

Figure 4: 2D colour maps of BrP from two design variations with a larger and a smaller avalanche region. BrP is shown at BV+4V and at 333K

To verify that the prediction of higher PDE for a smaller junction size is physical, we can extract the integrated PDE for a range of voltages. The resulting curve is shown for the three architectures with junctions of various widths overlaid by the appropriate experimental results in figure 5. The PDE values are obtained by multiplying the breakdown avalanche probability by an average optical absorption, found to be 26% for this architecture.
The comparison was extended to a large set of fifteen different architectures with electric field profiles selected for their wide range of electrostatic characteristics. As shown in figure 6, which presents the correlation between simulation and experiment at 4V excess voltage, the model was able to predict a significant range of PDE correctly.
An additional strength of the avalanche breakdown probability methodology is that the breakdown voltage (BV) can be extracted from the PDE vs voltage curve. We define that the device has broken down when a threshold PDE of $1e-5$ is reached, as shown in figure 7. The extraction was performed on the same fifteen diodes and the results, shown in figure 8, show the resulting correlation. In particular, the extreme breakdown voltages engineered for SPADs 3 and 4 are predicted by the model with ease.
Finally a comparison between characterisation and simulation was made for the jitter model. Figure 9 shows two diodes engineered to exhibit varying jitter profiles. In order to verify that jitter model is valid for a wide range of architectures, the pitch size and a variety of layout parameters were varied. The experimental results for the large diode show a strong initial peak and a rapid decrease in jitter. In contrast, the

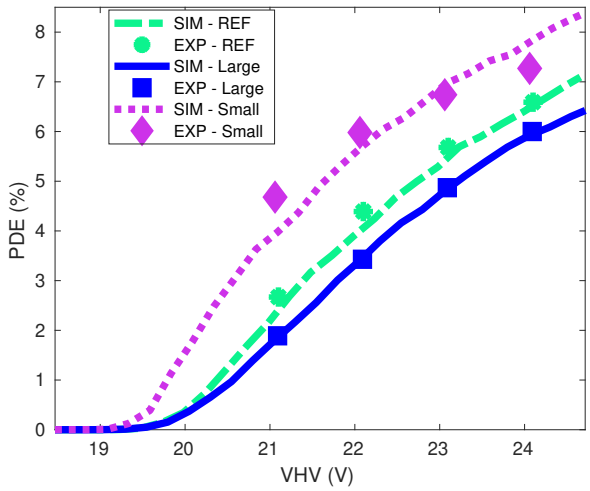

Figure 5: Comparison of PDE measured and simulated on three architecture variations

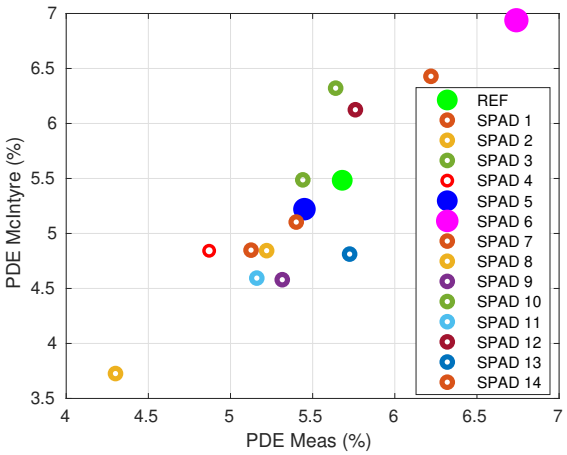

Figure 6: Correlation between simulation and experiment for PDE at BV+4V at 333K for 15 diodes of varying architecture

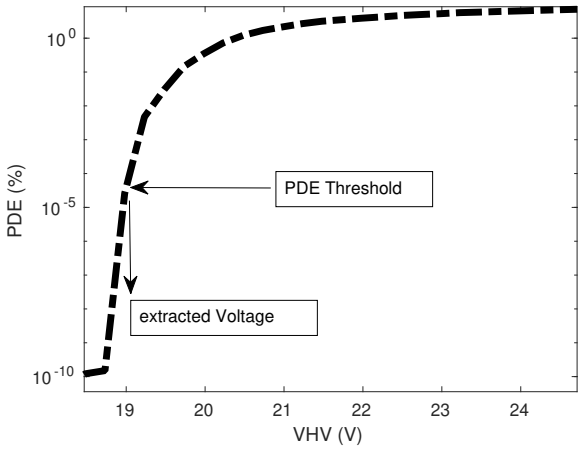

Figure 7: Method for BV extraction; the threshold defining breakdown is defined at a PDE of $1e-5$

smaller diode has a much weaker initial peak and a second smaller peak leading to a longer jitter tail. These characteristics are well represented in the simulation results, which shows a second peak for the smaller diode and longer tail. The crossing point between the two curves is also clearly indicated.

The good predictivity shown by both the BrP and jitter models in predicting PDE, BV and jitter characteristics is essential to confirm a clear understanding of the device physics. Furthermore, it allows for many iterations of design optimization without the need for silicon.

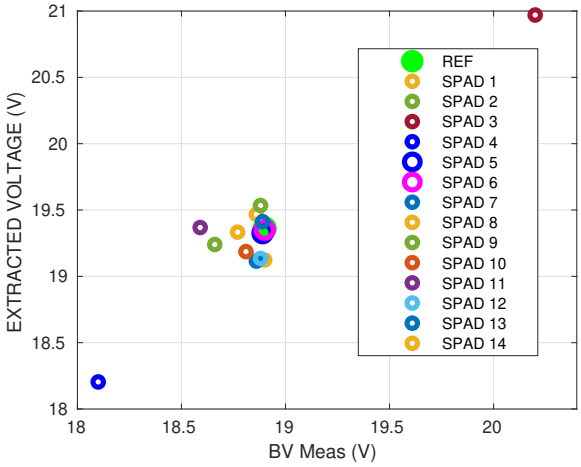

Figure 8: Correlation between simulation and measurements for BV at 333K for 15 diodes of varying architecture

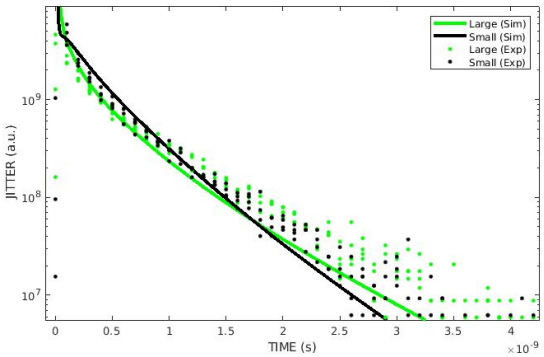

Figure 9: Comparison between characterisation and simulation for jitter on a 10um and 5um diode at BV+4V

References

[1] W. Oldham, R. Samuelson, and P. Antognetti, "Triggering phenomena in avalanche diodes," *IEEE Transactions on Electron Devices*, vol. 19, pp. 1056–1060, Sept. 1972.

[2] U. M. Ascher, R. M. M. Mattheij, and R. D. Russell, *Numerical Solution of Boundary Value Problems for Ordinary Differential Equations*. Philadelphia: Society for Industrial and Applied Mathematics, 1st edition ed., Jan. 1987.

[3] A. Panglosse, P. Martin-Gonthier, O. Marcelot, C. Virmontois, O. Saint-Pé, and P. Magnan, "Dark Count Rate Modeling in Single-Photon Avalanche Diodes," *IEEE Transactions on Circuits and Systems I: Regular Papers*, vol. 67, pp. 1507–1515, May 2020. Conference Name: IEEE Transactions on Circuits and Systems I: Regular Papers.

[4] R. Van Overstraeten and H. De Man, "Measurement of the ionization rates in diffused silicon p-n junctions," *Solid-State Electronics*, vol. 13, pp. 583–608, May 1970.